# FEC-Aided Decision Feedback Blind Mismatch Calibration of TIADCs in Wireless Time-Varying Channel Environments

Haoyang Shen, *Member, IEEE*, Deepu John, *Senior Member, IEEE*, and Barry Cardiff, *Senior Member, IEEE*

***Abstract*— Time-interleaved analog-to-digital converters (TIADCs) are widely used in communication systems due to their exceptionally high sampling rates; however, in real-world applications, the offset, gain, and time-skew mismatches in TIADCs are a significant challenge for the circuit system. This article proposes a forward error correction (FEC)-aided decision feedback blind mismatch calibration for TIADCs in the time-varying channels environment specific to the orthogonal frequency-division multiplexing (OFDM) system. In our proposed approach, we use an FEC decision feedback technique to generate a ground truth reference signal for the purpose of calibration. There are two stages. In the first stage, the offset and gain mismatches are estimated and corrected using standard techniques. In the second stage, an adaptive filter bank corrects the time-skew mismatch directly without the need for any additional calibration hardware. The coefficients of this adaptive filter are continuously adjusted in the background based on an error signal derived from the decision feedback ground truth signal. This calibration algorithm significantly reduces the bit error rate (BER) and improves the system performance. The efficacy of these approaches is validated through comprehensive simulations to attain a performance assessment, quantified by the BER, using a realistic wireless time-varying channel system configuration.**

***Index Terms*— Background calibration, forward error correction (FEC), low-density parity check (LDPC) code, orthogonal frequency-division multiplexing (OFDM), time-interleaved analog-to-digital converter (TIADC), time-varying channel, wireless communication.**

## I. Introduction

ORTHOGONAL frequency-division multiplexing (OFDM) is a common application for the time-varying channels in communication systems [1]. This technique necessitates the deployment of high-speed analog-to-digital converters (ADCs) at the receiving terminal due to its high data transmission rate; for example, time-interleaved ADCs (TIADCs) find extensive utilization in OFDM systems, see [2], [3], [4], [5], [6], [7]. The main challenge of TIADC is that the offset, gain, and time-skew mismatch due to its unique structure, and many circuit designers are focusing on developing the mismatch calibration algorithms in [8], [9], [10], [11], [12], [13], [14], [15], [16], [17], [18], and [19] to improve the system performance. In the time-varying environment, these mismatches will significantly affect the reliability of the whole system and reduce communication quality. The bit error rate (BER) evaluation for the OFDM system with the effect of TIADC mismatches are statistically analyzed in [5], [6], and [7].

The TIADC mismatch calibration is either foreground or background to address the mismatch issue. The foreground mismatch calibration [16], [20] knows the prior knowledge of the input signal to implement more accurate estimation and fast convergence. However, the main disadvantage of this calibration configuration is that it cannot monitor the changes caused by process, voltage, and temperature (PVT) [21] and adds the cost of interrupting the normal communication process. It is important to track the mismatch changes because the data are lost or corrupted during transmission, leading to errors in the received signal and reduced communication quality. Thus, the background calibration should be considered in the OFDM–TIADC system.

Many background calibration algorithms require knowledge of the input signal statistics and/or require additional (redundant) hardware [14], [17], [18], [19]. However, in many communication protocols, it is possible for the receiver (post error correction) to recreate a perfect local copy of the noise-free transmit signal by re-encoding the successfully decoded data packets, which could be used as a ground-truth signal [22] for the purpose of background ADC calibration. In wireless systems, the situation is further complicated by the presence of a time-varying channel between the transmitter and receiver, which also needs to be accounted for. To the best of the authors' knowledge, there is currently only limited work emphasis on the TIADC mismatch calibration in time-varying channel environments [2], [3], [4]. The work in [2] assumes knowing the perfect channel-state-information (CSI) in the receiver. Oh and Murmann [3] only address the interchannel offset mismatches using the pseudorandom modulation technique at the pilot tones. One limitation of this article [4] is that it assumes that the normalized timing error is limited within an interval (e.g., $[-0.2, 0.2]$).

For most digital TIADC calibration, there are two all-digital loop configurations, as shown in Fig. 1, which connect the estimation and correction sub-blocks [23]. The feedforward

Manuscript received 21 September 2023; revised 4 December 2023 and 2 January 2024; accepted 13 January 2024. Date of publication 1 February 2024; date of current version 28 June 2024. This work was supported in part by the China Scholarship Council and in part by the Microelectronic Circuits Centre Ireland. *(Corresponding author: Haoyang Shen.)*

The authors are with the School of Electrical and Electronic Engineering, University College Dublin, Dublin, D04 V1W8 Ireland (e-mail: haoyang.shen@ucdconnect.ie; deepu.john@ucd.ie; barry.cardiff@ucd.ie).

Color versions of one or more figures in this article are available at https://doi.org/10.1109/TVLSI.2024.3355316.

Digital Object Identifier 10.1109/TVLSI.2024.3355316

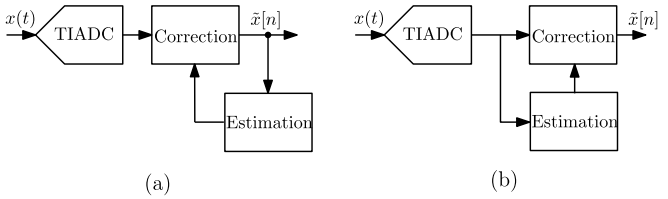


Fig. 1. Two loop configuration for TIADC. (a) All-digital feedback calibration structure. (b) All-digital feedforward calibration structure.

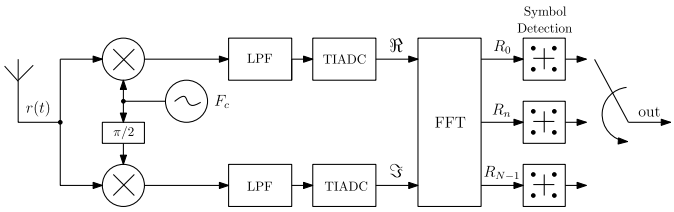


Fig. 2. OFDM receiver end structure with TIADC.

calibration structure [23], [24], [25] can avoid the possibility of system instability; nevertheless, it necessitates intensive computational procedures involving large divisions and multiplicative operations. In contrast, the feedback calibration in [14], [17], [26], and [27] can enhance the linearity of ADCs as the residues diminish upon convergence. This characteristic enables the introduction of additional approximations to the estimation mechanism without compromising the overall performance.

The low-density parity check (LDPC) codes are widely used for channel coding on the time-varying channel environments [28], [29], [30]. These codes have the ability to correct errors introduced by a noisy communication channel. In LDPC coding, a set of parity bits are produced by multiplying a matrix between a subset of the data bits and a parity check matrix. Any errors detected during the parity check are corrected by utilizing the information provided by the parity bits. Many communication applications [2], [31] use convolutional code as the forward error code (FEC) in time-varying channel environments. Compared with the convolutional coded system, the LDPC codes have parity bits that indicate whether this bits stream block is correct, which helps us to decide whether to update our system. They are also recognized for their superior error correction capability compared with convolutional codes [32].

This article proposes a novel background mismatch calibration of TIADC that uses the FEC-aided decision feedback technique to correct the offset, gain, and time-skew mismatch in the time-varying channels environment specific to the OFDM system. The FEC block uses the LDPC code to generate parity bits. When all parity bits are found to be 0, it is considered that the data contained within the symbol is correct. This information are then utilized to reconstruct the clean receiver signal and update the TIADC background mismatch calibration. Thus, we not only track the mismatch changes in transmission but also know the prior knowledge and input data. This method also has faster convergence and does not need any auxiliary ADCs and interruption operation.

In this work, the background calibration algorithm is divided into two stages. First, we estimate the values of offset and gain mismatches using the least-square estimation technique as we can obtain the clean version of the receiver signal from the update mechanism we proposed in this article. Compensating for offset and gain mismatches in the first stage, the time-skew mismatch can be treated as separate unknown systems for each sub-ADC, which can be achieved through the adaptive finite impulse response (FIR) filter bank. The coefficients of these FIR filters can be updated through the gradient descent algorithm by finding the minimum square error (MSE) object. As the desired signal can be reconstructed by utilizing the forward error correction (FEC) technique and the proposed system architecture, it eliminates the need for any auxiliary ADC, which results in a significant reduction in circuit area and power consumption.

The advantage of our proposed technique is that this blind calibration cannot be affected by some "pathological" input signals. Some previous background calibration algorithms [14], [15] may experience confusion when confronted with certain input signals, resulting in their inability to meet certain system performance requirements. The theoretical analysis of this scenario is presented in [20]. This FEC-aided feedback structure can address the possibility of system instability issues caused by the conventional feedback structure [23]. Also, our mismatch calibration algorithm does not need the time-skew estimation technique as we have prior knowledge of the input data from the FEC-aided structure, leading to a reduction in hardware resources, faster convergence time, and low-computational complexity.

This article is organized as follows: the proposed OFDM–TIADC system with the FEC-aided decision feedback blind mismatch calibration and mathematical analysis is presented in Section II. Section III proposes a digital mismatch calibration algorithm to estimate and correct the offset, gain, and time-skew mismatches. The simulation results are carried out by MATLAB and are presented in Section IV. Finally, the conclusion is summarized in Section V.

## II. OFDM and TIADC Models

Fig. 2 shows a conventional block diagram of an OFDM system using two TIADCs for real and imaginary parts, respectively, at the receiving end. Although TIADCs can achieve a higher data rate, they will suffer from various mismatches due to the structure. To address these issues, we propose a system in Fig. 3 to implement the FEC-aided decision feedback blind mismatch calibration that can track the mismatch change and update the mismatch calibration parameters in real time. The FEC block uses the LDPC technique that can determine if the system needs to be updated according to the parity check bits generated by the LDPC decoder. If the parity bits of this symbol are all 0, we assume that there is no bit error in this data stream, and we can recreate the input data using the same FEC, OFDM modulation, and channel model. This controlled feedback structure can avoid the instability of conventional feedback calibration.

From Fig. 3, we define the quadrature modulation [e.g., phase shift keying (PSK) and quadrature amplitude modulation (QAM)] signal as $X_k$, which is the bits stream that goes through the FEC encode and mapping block. The output of

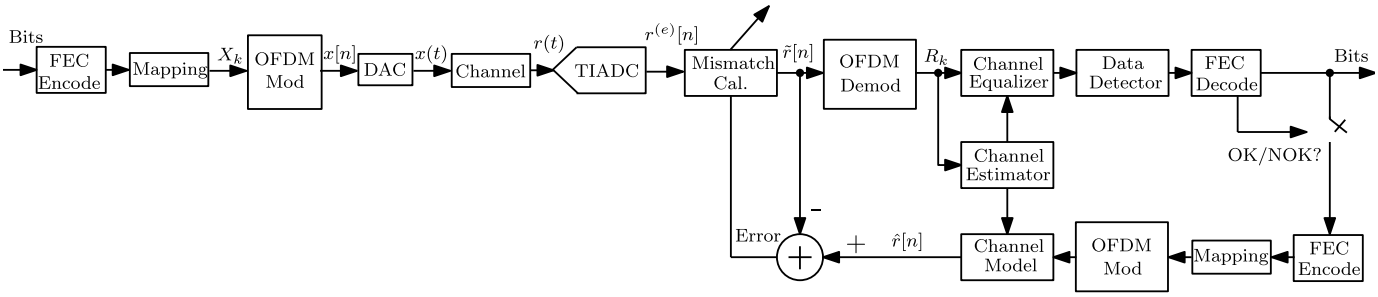


Fig. 3. FEC-aided decision feedback blind TIADC mismatch calibration in the OFDM system.

the OFDM modulation can be denoted by $x[n]$, which can be expressed as follows:

$$x[n] \triangleq \frac{1}{N}\sum_{k=0}^{N-1} X_k e^{\frac{j2\pi kn}{N}} \tag{1}$$

where $N$ is the number of subcarriers in the OFDM modulation.

We define $h(t)$ as the impulse response of the time-varying multipath fading channel and $T$ as the sampling time of the TIADC. The signal at the receiver is the convolution of the transmit signal and the channel impulse response in [33] and plus an additive white Gaussian noise (AWGN) component, $\eta(t)$ and can be expressed as follows:

$$\begin{aligned} r(t) &= \sum_{n=0}^{N-1} x(t)h(t-nT) + \eta(t) \\ &= \frac{1}{N}\sum_{k=0}^{N-1} X_k e^{\frac{j2\pi kt}{NT}} \sum_{n=0}^{N-1} h(t-nT)e^{-\frac{j2\pi k(t-nT)}{NT}} + \eta(t) \end{aligned} \tag{2}$$

where $\eta(t)$ is a Gaussian random variable with all samples independently and identically distributed (i.i.d.) and having noise spectral density $N_0$.

Although the fading channel is time varying, it can be considered as static for a single OFDM symbol in [33]. Consequently, we transform (2) in the frequency domain as follows:

$$r(t) = \frac{1}{N}\sum_{k=0}^{N-1} X_k H_k e^{\frac{j2\pi kt}{NT}} + \eta(t) \tag{3}$$

where $H_k$ represents the impulse response of the fading channel in the frequency domain for the $k$th OFDM symbol.

The receiver signal is divided into in-phase ($I$) and quadrature-phase ($Q$) components to be processed, as shown in Fig. 2 and we sample the $I$ and $Q$ waveforms using two TIADCs with the offset, gain, and time-skew mismatch sets defined as $\{(o_{I,n}, g_{I,n}, \tau_{I,n})\}$ and $\{(o_{Q,n}, g_{Q,n}, \tau_{Q,n})\}$, respectively; thus, the TIADC samples with mismatch of $I$ and $Q$ signal can be written as follows:

$$r_I^{(e)}[n] \triangleq \frac{1+g_{I,n}}{N}\sum_{k=0}^{N-1} \Re\left(X_k H_k e^{\frac{j2\pi k\left(n+\tau_{I,n}\right)}{N}}\right) + o_{I,n} \tag{4}$$

$$r_Q^{(e)}[n] \triangleq \frac{1+g_{Q,n}}{N}\sum_{k=0}^{N-1} \Im\left(X_k H_k e^{\frac{j2\pi k\left(n+\tau_{Q,n}\right)}{N}}\right) + o_{Q,n}. \tag{5}$$

Using complex notation, we have

$$r^{(e)}[n] \triangleq r_I^{(e)}[n] + jr_Q^{(e)}[n]. \tag{6}$$

Likewise, we can define $r[n]$ as the ideal sampled complex valued TIADC outputs based on (3). We observe from (4) and (5) that the offset mismatch is independent of $r(t)$, which makes it possible to estimate the offset values using the least-square technique. The presence of gain and time-skew mismatch results in signal-dependent interference, causing the received signal complex and having a combined impact on the signal. Thus, we use an all-digital background calibration by first estimating and correcting the offset and gain mismatches and designing the adaptive filter bank to correct the time-skew mismatch. The details of our proposed calibration algorithm are presented in Section III.

## III. Mismatch Calibration

This section proposes a two-stage decision feedback blind mismatch calibration that first estimates and corrects the offset and gain mismatch simultaneously then corrects the time-skew problem using the adaptive filter bank. As the interference caused by the combined impact of the gain and time-skew mismatch is tiny, we neglect the time-skew mismatch in the first stage.

### A. Offset and Gain Mismatches

Rewriting (6) in a vector form we have

$$\boldsymbol{r}^{(\boldsymbol{e})} = \frac{1}{2}\left(\left(\boldsymbol{\Delta}_I + \boldsymbol{\Delta}_Q\right) + \left(\boldsymbol{\Delta}_I^* - \boldsymbol{\Delta}_Q^*\right)\right)\boldsymbol{r} + \boldsymbol{o} + \boldsymbol{\eta} \tag{7}$$

where we have the elements of the vectors $\boldsymbol{\Delta}_I$ and $\boldsymbol{\Delta}_Q$ as follows:

$$\Delta_I[n] \triangleq \frac{1+g_{I,n}}{N}\sum_{k=0}^{N-1} e^{\frac{j2\pi k\tau_{I,n}}{N}}$$

$$\Delta_Q[n] \triangleq \frac{1+g_{Q,n}}{N}\sum_{k=0}^{N-1} e^{\frac{j2\pi k\tau_{Q,n}}{N}}$$

respectively. When the FEC decoder indicates that it has (with high likelihood) generated correct decisions, we recreate the input data which we define as $\hat{r}[n]$ as shown with the ok/nok switch in Fig. 3. We can then compute the following:

$$\zeta_I[n] \triangleq \frac{\Re\{r^e[n]\}}{\Re\{\hat{r}[n]\}} \quad \text{and} \quad \zeta_Q[n] \triangleq \frac{\Im\{r^e[n]\}}{\Im\{\hat{r}[n]\}}. \tag{8}$$

Neglecting the time-skew mismatch temporarily, the values establish a relationship with the offset and gain mismatches can be written as follows:

$$\begin{cases} \zeta_I[n] = 1 + g_{\{I,n\}} + \dfrac{o_{\{I,n\}}}{\Re\{\hat{r}[n]\}} + \epsilon_{_I}[n] \\ \zeta_Q[n] = 1 + g_{\{Q,n\}} + \dfrac{o_{\{Q,n\}}}{\Im\{\hat{r}[n]\}} + \epsilon_{_Q}[n] \end{cases} \tag{9}$$

where $\epsilon_{_I}[n]$ and $\epsilon_{_Q}[n]$ are considered to be an AWGN contribution.

Using the $I$ signal as an example, (9) can be expressed using the matrix form as follows:

$$\boldsymbol{\zeta}_I = \left[ \boldsymbol{Q} \middle| \operatorname{diag}\left\{ \frac{1}{\Re\{\hat{r}[n]\}} \right\} \boldsymbol{Q} \right] \begin{bmatrix} \boldsymbol{g}_I + \mathbf{1} \\ \boldsymbol{o}_I \end{bmatrix} \tag{10}$$

where $\boldsymbol{g}_I$ and $\boldsymbol{o}_I$ are vectorized[1] versions of $g_{\{I,n\}}$ and $o_{\{I,n\}}$ respectively, and $\boldsymbol{Q}$ is defined as a matrix with $N \times M$ dimension combined by $N$ identity matrix of size $M$ as follows:

$$\boldsymbol{Q} \triangleq \begin{bmatrix} \boldsymbol{I}_M \\ \hline \boldsymbol{I}_M \\ \hline \vdots \\ \hline \boldsymbol{I}_M \end{bmatrix}.$$

Note that for mathematical stability reasons we either remove or set to 0 the rows[2] in (10) where the value of $\Re\{\hat{r}[n]\} \approx 0$ However, as this condition is ambiguous, in practice, we remove/zero the rows where $\Re\{\hat{r}[n]\} < \Im\{\hat{r}[n]\}$.

From (10), we can apply a pseudoinverse to obtain estimates $\tilde{\boldsymbol{g}}_I$ and $\tilde{\boldsymbol{o}}_I$ for $\boldsymbol{g}_I$ and $\boldsymbol{o}_I$, respectively, as follows:

$$\begin{bmatrix} \tilde{\boldsymbol{g}}_I + \mathbf{1} \\ \tilde{\boldsymbol{o}}_I \end{bmatrix} = \left[ \boldsymbol{Q} \middle| \operatorname{diag}\left\{ \frac{1}{\Re\{\hat{r}[n]\}} \right\} \boldsymbol{Q} \right]^{\dagger} \boldsymbol{\zeta}. \tag{11}$$

Likewise, starting with $\zeta_Q[n]$ estimates $\tilde{\boldsymbol{g}}_Q$ and $\tilde{\boldsymbol{o}}_Q$ can be derived by interchanging the roles of $I$ and $Q$ is the above procedure.[3] If the offset and gain mismatch changes, the correct values will be updated with the help of the decision feedback structure using (11).

### B. Time-Skew Mismatch

We propose an adaptive FIR filter bank to do the timing error correction directly without any time-skew estimation techniques. Usually, to implement this, we need an auxiliary ADC as the reference to get the coefficient of the adaptive filter bank; however, in our decision feedback structure, we can recreate the input signal as the reference without any auxiliary circuits, which reduces the area of the circuit and also provides a faster convergence time and avoids instability issue. Another advantage of this method is that the architecture does not need intensive computations as we do not have the time-skew estimation block.

We estimate and compensate for the offset and gain mismatches in the first stage. Next, we present the time-skew mismatch calibration for the second stage. We define the TIADC output with offset and gain mismatch free as $y[n]$ and (7) can be rewritten as follows:

$$\begin{aligned} y[n] &= \frac{\Re\{r^{(e)}[n] - \tilde{o}[n]\}}{\Re\{\tilde{g}[n]\} + 1} + j\left( \frac{\Im\{r^{(e)}[n] - \tilde{o}[n]\}}{\Im\{\tilde{g}[n]\} + 1} \right) \\ &= \frac{\Re\{r[n]\}}{N} \sum_{k=0}^{N-1} e^{\frac{j2\pi k \tau_{I,n}}{N}} + j\left( \frac{\Im\{r[n]\}}{N} \sum_{k=0}^{N-1} e^{\frac{j2\pi k \tau_{Q,n}}{N}} \right). \end{aligned} \tag{12}$$

For the time-skew mismatch calibration, we consider the signal as in-phase ($I$) and quadrature-phase ($Q$) components separately, which can be written as follows:

$$\boldsymbol{y_I} = \frac{\Re\{\boldsymbol{r}\}}{N} \sum_{k=0}^{N-1} e^{\frac{j2\pi k \tau_{I,n}}{N}} + \boldsymbol{\eta} \tag{13}$$

$$\boldsymbol{y_Q} = \frac{\Im\{\boldsymbol{r}\}}{N} \sum_{k=0}^{N-1} e^{\frac{j2\pi k \tau_{Q,n}}{N}} + \boldsymbol{\eta}. \tag{14}$$

Using the in-phase signal as an example, the precise timing error values of individual sub-ADCs are not considered; instead, they are treated as separate unknown systems, $H_m$. Using one sub-ADC as an example, we consider an adaptive filter defined as $P$ to implement the inverse system of $H$. Fig. 4 depicts the time-skew mismatch correction by the minimum mean-squared error (MMSE) method.

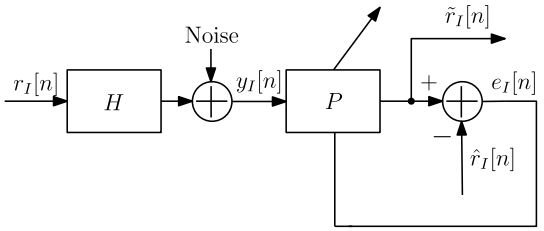


Fig. 4. Block diagram of the one sub-ADC's time-skew correction for the in-phase signal as an example. Using the MMSE estimator to inverse the unknown system, $H$, where $\hat{r}_I[n]$ is from the decision feedback technique.

To get the inverse system, $P$, we estimate the filter coefficients by minimizing the MSE and by utilizing the statistical characteristics. In Fig. 4, for the in-phase signal, we define the noise-free input as $r_I[n]$ and the corrected output signal as $\tilde{r}_I[n]$, which can be written as follows:

$$\tilde{r}_I[n] = \sum_{l=0}^{L-1} p[l] y_I[n-k] \tag{15}$$

where $L$ is the length of the adaptive filter.

The MSE of the inverse system can be written as follows:

$$\begin{aligned} J_{\text{MSE}}(\boldsymbol{p}) &= \mathbb{E}\left\{ \left( \hat{r}_I[n] - \tilde{r}_I[n] \right)^2 \right\} \\ &= \mathbb{E}\left\{ \left( \hat{r}_I[n] - \boldsymbol{p}^{\mathrm{T}} \boldsymbol{y_I}[\boldsymbol{n}] \right)^2 \right\} \\ &= \mathbb{E}\{\hat{r}_I^2[n]\} - 2\boldsymbol{p}^{\mathrm{T}} \mathbb{E}\{\hat{r}_I[n] \boldsymbol{y_I}[\boldsymbol{n}]\} \\ &\quad + \boldsymbol{p}^{\mathrm{T}} \mathbb{E}\{\boldsymbol{y_I}[\boldsymbol{n}] \boldsymbol{y_I}[\boldsymbol{n}]^{\mathrm{T}}\} \boldsymbol{p} \end{aligned} \tag{16}$$

where $\boldsymbol{p} \triangleq \left[ p[0], \ldots, p[l], \ldots, p[L-1] \right]^{\mathrm{T}}$ and $\boldsymbol{y_I}[\boldsymbol{n}] \triangleq \left[ y_I[n], \ldots, y_I[n-l], \ldots, y_I[n-(L-1)] \right]^{\mathrm{T}}$.

[1]Unless otherwise stated, all vectors are column vectors.

[2]Both options are equivalent, and the choice is based on implementation preference.

[3]Now, the rule for removing/zeroing rows becomes $\Im\{\hat{r}[n]\} < \Re\{\hat{r}[n]\}$.

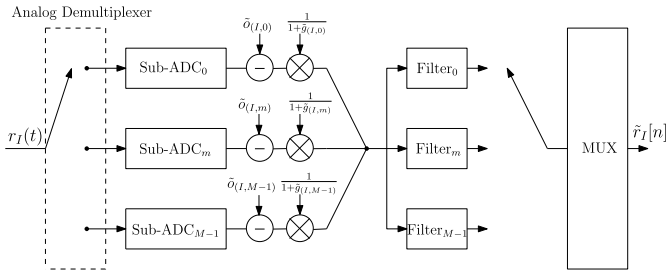


Fig. 5. $M$-channel TIADC mismatch calibration correction diagram.

TABLE I
CELL-WIDE SETTINGS

| Parameters | values | Description |
|---|---|---|
| NDLRB | 15 | Number of downlink resource blocks |
| NCellID | 10 | Physical layer cell identity |
| CellRefP | 1 | The number of cell-specific reference signal |
| CyclicPrefix | Normal | Cyclic prefix length |
| DuplexMode | FDD | Duplexing mode, specified Frequency Division Duplex |

TABLE II
RAYLEIGH FADING MODEL CONFIGURATION

| Parameters | Values | Description |
|---|---|---|
| NRxAnts | 1 | Number of receive antennas |
| MIMOCorrelation | Low | The correlation between UE and eNodeB antennas |
| DelayProfile | EVA | Extended Vehicular A model [35] |
| DopplerFreq | 70 Hz | Maximum Doppler frequency |
| NTerms | 16 | The number of oscillators employed in fading channels |
| ModelType | GMEDS | The Rayleigh fading is modeled as Generalized Method of Exact Doppler Spread [38] |
| NormalizePathGains | On | The model output is normalized |

To find the minimum value of (16), we consider the gradient descent algorithm. The gradient of (16) can be expressed as follows:

$$\nabla J_{\mathrm{MSE}}(\boldsymbol{p}) = -2\mathbb{E}\{\hat{r}_I[n]\boldsymbol{y_I}[\boldsymbol{n}]\} + 2\mathbb{E}\{\boldsymbol{y_I}[\boldsymbol{n}]\boldsymbol{y_I}[\boldsymbol{n}]^{\mathrm{T}}\}\boldsymbol{p}. \quad (17)$$

The filter coefficients of the system, $P$, can be solved for $\boldsymbol{p}$ to express as follows:

$$\boldsymbol{p} = \left(\mathbb{E}\{\boldsymbol{y_I}[\boldsymbol{n}]\boldsymbol{y_I}[\boldsymbol{n}]^{\mathrm{T}}\}\right)^{-1}\mathbb{E}\{\hat{r}_I[n]\boldsymbol{y_I}[\boldsymbol{n}]\}. \quad (18)$$

The MSE objective function (16) is quadratic, which guarantees it has a unique minimum value making the equation convergence. To find the desired result, a gradient descent algorithm is used as follows:

$$\begin{aligned}\boldsymbol{p}[\boldsymbol{n+1}] &= \boldsymbol{p}[\boldsymbol{n}] - \mu\left(\boldsymbol{y_I}[\boldsymbol{n}]\boldsymbol{y_I}[\boldsymbol{n}]^{\mathrm{T}}\boldsymbol{p}[\boldsymbol{n}] - \hat{r}_I[n]\boldsymbol{y_I}[\boldsymbol{n}]\right)\\ &= \boldsymbol{p}[\boldsymbol{n}] - \mu\left(\boldsymbol{y_I}[\boldsymbol{n}]\tilde{r}_I[n] - \hat{r}_I[n]\boldsymbol{y_I}[\boldsymbol{n}]\right)\\ &= \boldsymbol{p}[\boldsymbol{n}] - \mu(e[n]\boldsymbol{y_I}[\boldsymbol{n}]) \end{aligned} \quad (19)$$

where $\mu$ is the learning rate for the adaptation process.

Likewise, the other adaptive filters for the rest of the sub-ADC and the quadrature-phase components' adaptive filter bank can be implemented similarly. If the time-skew mismatch changes, the coefficient of adaptive filters will be re-convergence to track these changes.

TABLE III
CHANNEL ESTIMATOR CONFIGURATION

| Parameters | Values | Description |
|---|---|---|
| PilotAverage | 'UserDefined' | Type of pilot averaging |
| FreqWindow | 9 | Size of window for frequency averaging in resource elements |
| TimeWindow | 9 | Size of window for time averaging in resource elements |
| InterpType | 'Cubic' | Type of interpolation between pilot symbols |
| InterpWinSize | 3 | Interpolation window size, in number of subframes |
| InterpWindow | 'Centred' | Interpolation type |

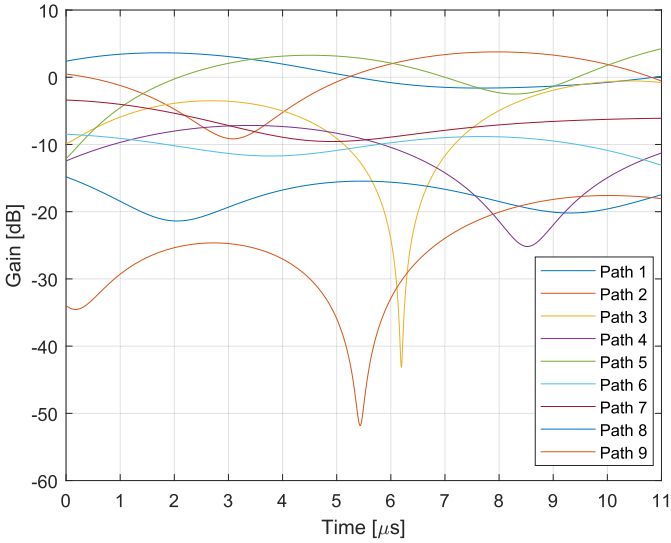


Fig. 6. Multipath channel gain for the Rayleigh fading channel with an EVA delay profile and 70-Hz Doppler frequency.

### C. Mismatch Correction

As we can get the coefficients of the adaptive filter bank, Fig. 5 depicts an example of the complete TIADC correction structure in the run-time process for in-phase signal. The addition and multiplication operations can implement the offset and gain mismatches correction according to estimation values from (11). The adaptive filter bank is employed to correct time-skew. It operates by decomposing the input signal into multiple sub-band components, processing each individually, and recombining them to generate a modified version of the original signal.

## IV. RESULTS

### A. Communication System Configuration

The results are obtained using a four-channel TIADC in the time-varying environment via MATLAB. The OFDM cell-wide setting parameters are displayed in Table I. In the simulation, only one transmit antenna is used, and the OFDM executes the insertion for the dc subcarrier, inverse fast Fourier transform (IFFT), and cyclic prefix insertion. Table II depicts the Rayleigh fading model configuration. We use the Extended Vehicular A model (EVA) 70-Hz delay profile [34] for the multipath fading channel model. In this delay profile, the highest Doppler frequency has been prescribed to be 70 Hz

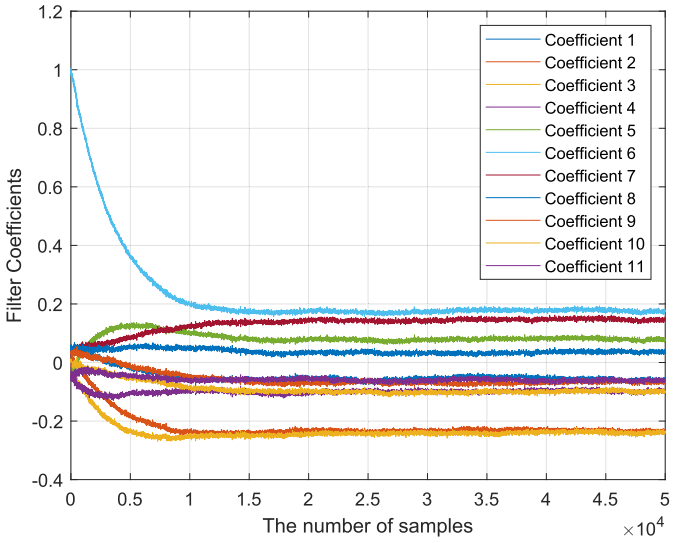


Fig. 7. Example of the convergence curves of adaptive filter coefficients of the sub-$ADC_1$.

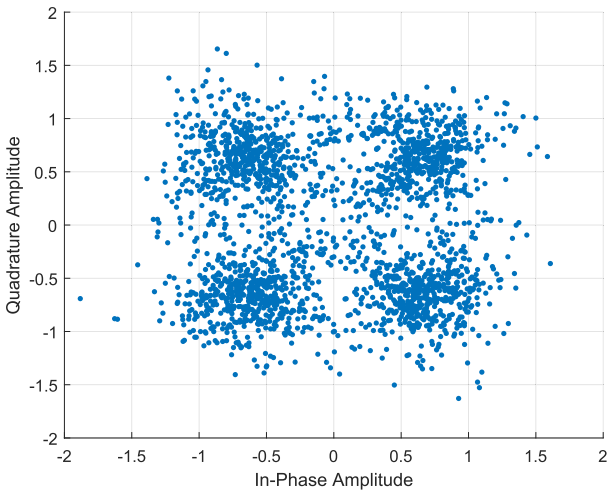


Fig. 8. Scatter diagram of QPSK modulation without TIADC calibration technique in the absence of AWGN.

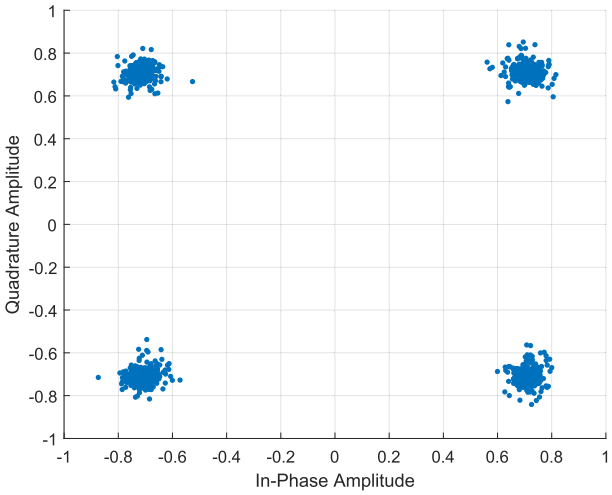


Fig. 9. Same scatter diagram as shown in Fig. 8 but with mismatch calibration algorithm.

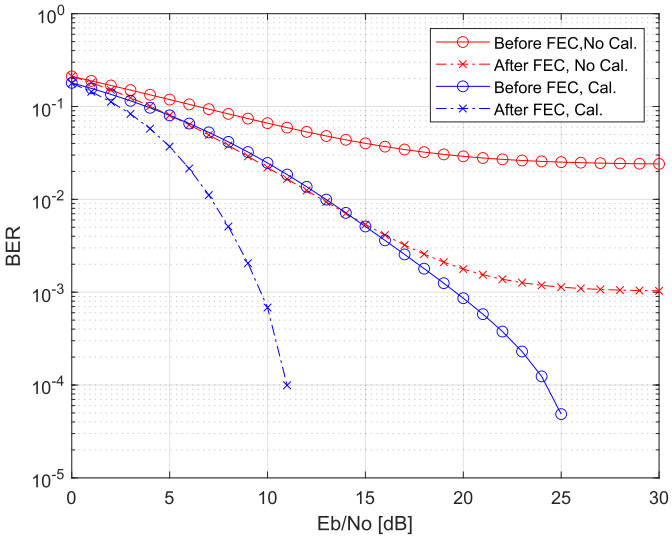


Fig. 10. BER with/without TIADC calibration for OFDM system before/after the LDPC decoder.

for all propagation scenarios that involve multipath fading. Usually, this delay profile represents a medium delay spread environment. Fig. 6 depicts the multipath channel gain for the Rayleigh fading channel from Table II.

The channel estimator configuration is presented in Table III. The parameter called "PilotAverage" is the type of pilot averaging. We used a user-defined window with $9 \times 9$ size and centered interpolation to reduce the effect of noise. van de Beek et al. [35] present a methodological approach for deriving least square estimates on the channel frequency response, specifically focusing on pilot symbols. To address the potential interpolation challenges arising from the absence of pilot symbols at the subframe edge, we introduce the concept of virtual pilot symbols. Consequently, the comprehensive estimation of the entire subframe is realized through the strategic utilization of interpolation techniques.

We use the LDPC coder with $1/2$ rate at the transmitter. The parity check matrix is from 802.16e [36]. Generally speaking, in any coder technique, a higher code rate implies fewer parity bits, potentially resulting in decreased error correction capabilities. Depending on the channel environment, the code rate will affect the package error rate (PER). In our algorithm, the calibration's effectiveness depends on the PER. When the PER is low, the proposed calibration algorithm continuously updates, leading to faster convergence. The higher layers of the protocol will select a code rate to suit the environment so as to target some quality of service (max allowable PER). Provided the PER is low, then our proposed algorithm will be given plenty of opportunity to update. In an example, using the rate $1/2$ code, the encoded block size is 11 760 bits with 5880 data bits and 5880 parity bits. If all parity bits are 0, we assume that all data bits are correct and do the mismatch calibration update, as shown in Fig. 3. We use a four-channel 12-bit TIADC instance with the normalized offset, gain, and time-skew mismatch errors were each drawn from zero mean Gaussian distributions each having a standard deviation of 0.2. The BER evaluation related to the standard deviation of TIADC mismatches is presented in [5], [6], and [7].

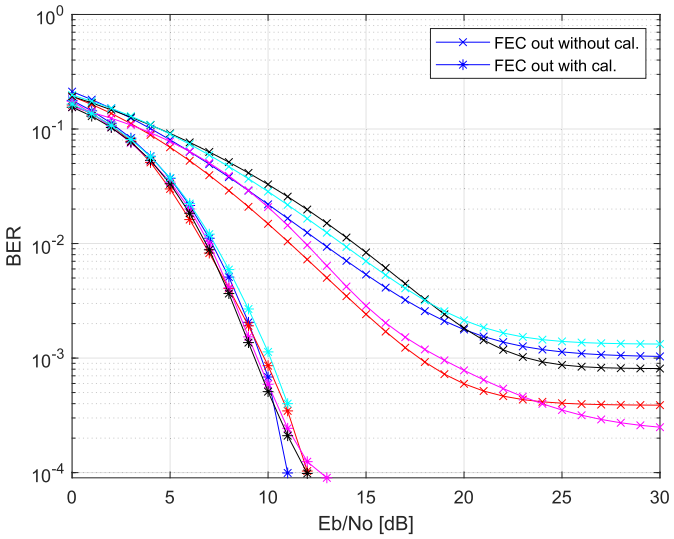


Fig. 11. BER of the data after the LDPC decoder without ("-×")/with ('-∗") TIADC mismatch calibration for five different TIADC instances. The fading channel with an EVA delay profile and 70-Hz Doppler frequency.

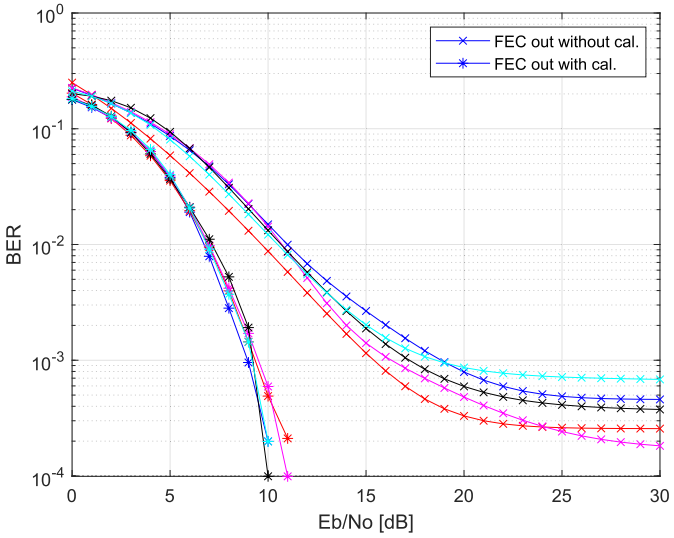


Fig. 12. Same TIADC instances as shown in Fig. 11 but with 5-Hz Doppler frequency.

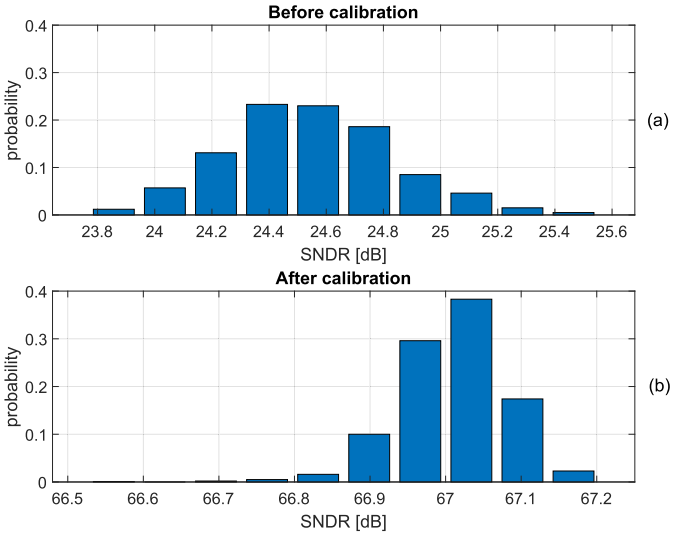


Fig. 13. SNDR performance for different 12-bit TIADC instances in Monte-Carlo simulation. (a) Before calibration. (b) After calibration.

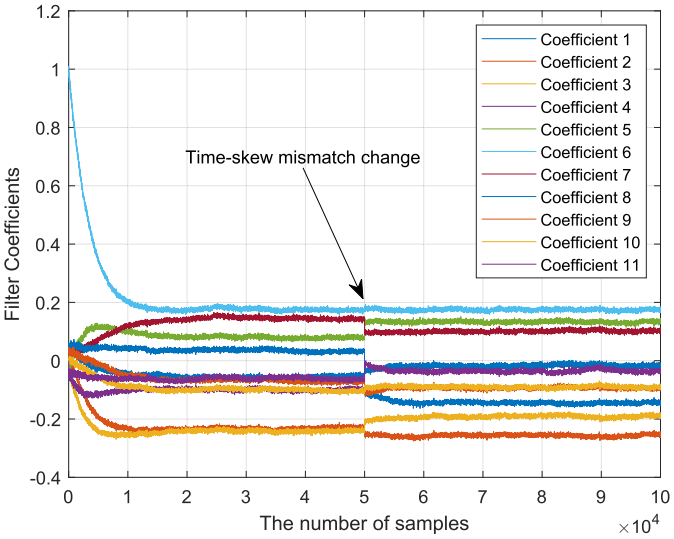


Fig. 14. Example of tracking the time-skew change. When the time-skew parameter undergoes a step change, the adaptive filter can track this change and quickly reconverge the coefficients.

### B. Calibration Algorithm Tests

Using sub-ADC$_1$ as an example, Fig. 7 depicts the convergence curves of the coefficients of the adaptive FIR filter. From this figure, we can see that the convergence time is $50k$ samples.

We use quadrature phase shift keying (QPSK) modulation in each subcarrier. Without TIADC mismatch calibration, the scatter diagram of the transmitting data after the channel equalizer is shown in Fig. 8. Fig. 9 depicts the scatter diagram of the channel equalizer results with the proposed mismatch calibration. As expected, the constellation results are much better during the mismatch calibration work.

Fig. 10 depicts the measured BER result of the decision feedback blind calibration algorithm for a four-channel TIADC in the time-varying environment with the QPSK modulation before/after the LDPC decoder. When we disable the mismatch calibration, the TIADC mismatches seriously affect the system performance even at high SNRs, and the bit error cannot be fully corrected by the LDPC decoder as shown in two different red lines labeled "No Cal." in Fig. 10. When we enable the mismatch calibration, as the blue lines labeled "Cal." As shown in Fig. 10, the BER significantly reduces in the OFDM system, and the error floor is removed after the LDPC decoder.

### C. Robustness Tests

Fig. 11 depicts the output of the LDPC decoder without/with TIADC mismatch calibration algorithm for five different four-channel TIADC instances. Each TIADC instance has the same ADC architecture and the same standard deviation of Gaussian distributions for offset, gain, and time-skew but varying mismatch values. As expected, the proposed background calibration algorithm is robust for different TIADC instances and significantly improves the system performance. Fig. 12 does the same simulation but with a 5-Hz Doppler frequency

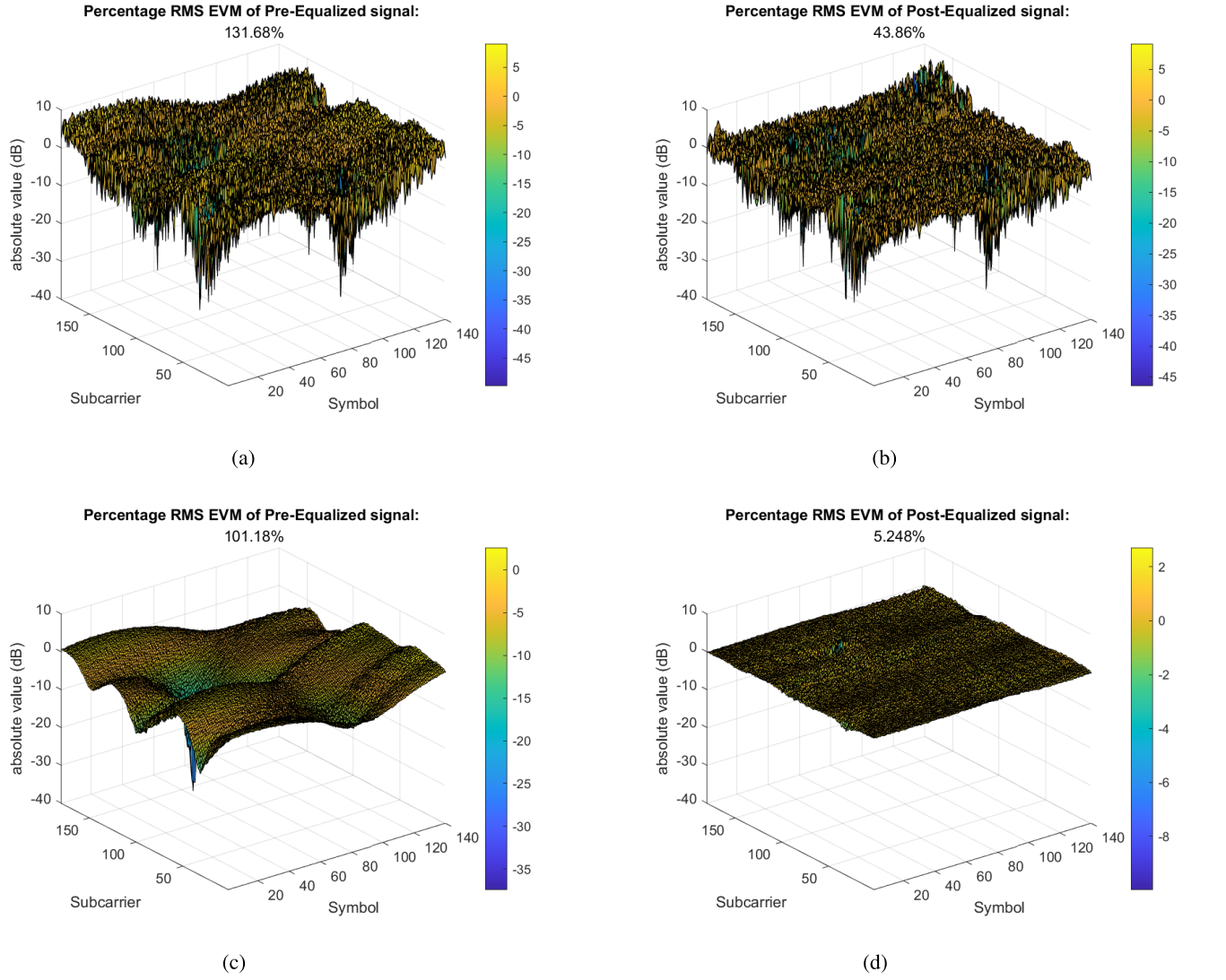


Fig. 15. Percentage rms EVM of pre-equalized/postequalized without/with TIADC calibration technique. (a) Pre-equalized without TIADC calibration. (b) Postequalized without TIADC calibration. (c) Pre-equalized with TIADC calibration. (d) Postequalized with TIADC calibration.

for the EVA delay profile. It is clear that our mismatch calibration technique is reliable in any scenario.

In our simulation environment, we know what TIADC input is from the receiver; thus, we can create noise-free TIADC outputs to compute the signal power and noise power for Signal-to-Noise and Distortion Ratio (SNDR) evaluation before/after mismatch calibration. To present the TIADC performance, we use the Monte-Carlo simulation to test 1000 TIADC instances with the same architecture and standard deviation of mismatches but varying offset, gain, and time-skew mismatch values. To reduce the simulation time, we use the perfect CSI and perfect local copy (only available in the simulation environment) to converge the mismatch calibration algorithm and correct the offset, gain, and time-skew mismatches. Fig. 13(a) and (b) depicts the SNDR for TIADC without calibration algorithm and the SNDR for TIADC after mismatch calibration algorithm, respectively. It is seen that our algorithm achieves a significant SNDR improvement for TIADC in this wireless communication system.

As we mentioned, one advantage of our proposed mismatch calibration is that it can track mismatch changes. To prove this, we create an artificial scenario as shown in Fig. 14 where the time-skew parameter values undergo a step change (perhaps due to some sudden environmental change), and we see the estimated parameters respond to this change naturally. It is seen that when we change the time-skew mismatch in the simulation, the adaptive filter can track this change and quickly reconverge the coefficients, which proves our algorithm can track the time-skew mismatch change. The same can be said for the gain and offset mismatches.

### D. EVM Evaluation and Channel Estimation

Fig. 15 presents the percentage root mean square (rms) error vector magnitude (EVM) of pre-equalized and postequalized signals disabled and enabled the calibration algorithm for TIADC mismatch. Before the mismatch calibration, the percentage rms EVM of pre-equalized and postequalized signals are 131.68% and 43.86%, respectively. After the mismatch calibration algorithm, the results for the pre-equalized and postequalized signals are 101.18% and 5.25%, respectively. The EVM has significantly reduced when the mismatch

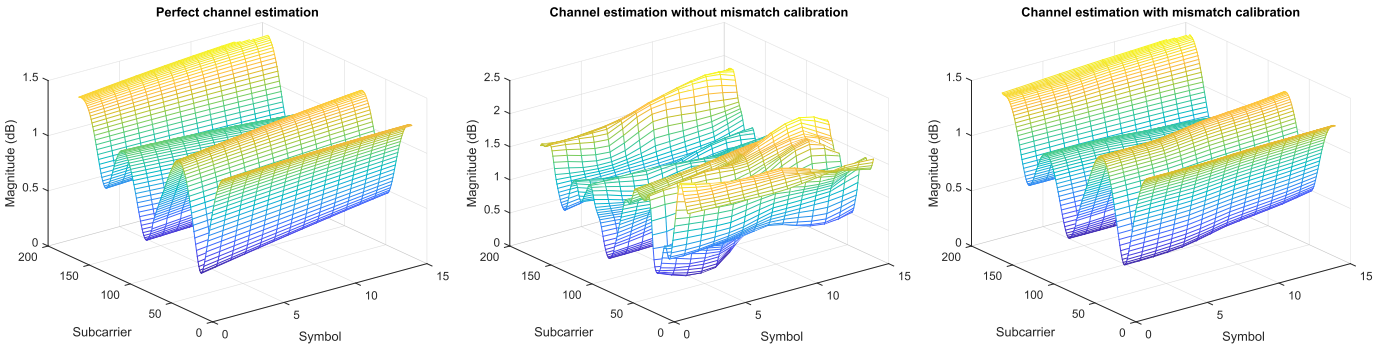


Fig. 16. (a) Perfect channel estimation. (b) Channel estimation without mismatch calibration (note different vertical scales). (c) Channel estimation with mismatch calibration.

TABLE IV
COMPARISON OF OUR TIME-SKEW MISMATCH CALIBRATION WITH OTHER PRIOR TIME-SKEW CALIBRATION TECHNIQUES

| **Characteristics** | **[12] 2021 TVLSI** | **[13] 2023 TVLSI** | **[14] 2018 TCAS-I** | **[17] 2022 TCAS-I** | **This work** |
|---|---|---|---|---|---|
| **Calibration routine** | Background | Background | Background | Background | Background |
| **Configuration** | Feedforward | Feedback | Feedback | Feedback | Feedback |
| **Number of sub-ADC** | 4 | 4 | $M$ | 4 | 4 |
| **Time-skew Estimation** | Correlation-based | Parallel Correlation Derivative | Spur construction + LMS | Modulation matrix | - |
| **Time-skew Correction** | VDLs | Derivative filter | Adaptive filter | Derivative filter | Adaptive filter |
| **Conv. Time (Samples #)** | $204.8K$ | $524.29K$ | $400K$ | $110K$ | $50K$ |
| **Adder #** | $3M+3$ | - | $(2L_h+4)+L-1$ | $4(M-1)$ $+1+L-1$ | $L-1$ |
| **Multiplier #** | $3M+2$ | - | $(2L_h+8)+L$ | $2(M-1)$ $+1+L$ | $L$ |

1. $M$ is the number of sub-ADC.
2. $L$ is the length of the FIR filter, $L_h$ is the length of the Hilbert filter.

calibration was enabled. The outcome of the postequalized signal is consistent with our initial expectations and demonstrates satisfactory performance. Fig. 16 presents the channel estimation result. Fig. 16(a) depicts the perfect channel estimation which we can obtain from the channel information and from the channel simulation configuration. Fig. 16(b) shows the channel estimation without mismatch calibration and the outcome exhibits significant inadequacy. Fig. 16(c) presents the channel estimation outcome exhibits a high level of agreement with the ideal results, as shown in Fig. 16(a).

### *E. Comparison of the Prior Works*

The time-skew mismatch is the most considered in the TIADC mismatch calibration. Table IV presents the comparative results between the proposed work and the other state-of-the-art background calibration techniques addressing time-skew mismatches for TIADCs. The main advantage of our work is that we do not need the time-skew estimation technique as we know the prior knowledge of the input data to train the adaptive filter bank, efficiently reducing the hardware resources. The other methods, for example, the correlation-based estimation [12], [13], the LMS in [14], and the modulation matrix in [17] will introduce the intensive computation in the estimation technique, which may affect the processing time in hardware implementation. Also, our adaptive filters have a faster convergence time, 50$k$ samples, much less than the other methods in Table IV. Although the time-skew mismatch is the most considerable by prior works [9], [10], [11], [12], [13], we still compare our work to other methods in [18] and [19] addressing all three mismatches to make our analysis more comprehensive. Compared with these works, the main advantage of our proposed algorithm is that we use one least-square technique to estimate the offset and gain mismatch simultaneously to reduce the circuit area.

## V. CONCLUSION

This article presents a novel FEC-aided decision feedback blind mismatch calibration of TIADC in the time-varying channel environment and verifies it in the TIADC–OFDM system. The proposed system structure employs LDPC code in the FEC block to detect and correct bit errors during the transmission. Moreover, a two-stage background joint mismatches calibration technique is proposed, which employs least-square estimation for offset and gain mismatches and an MMSE algorithm to train the adaptive filter bank for time-skew mismatch correction. Due to the advantage of the FEC-aided decision feedback technique, our system does not have the instability issue as the conventional feedback calibration structure. This algorithm can also track the mismatch

changes and know the prior knowledge of input data to increase the convergence speed. The time-skew calibration stage does not need an auxiliary ADC or time-skew estimation algorithm to implement the timing error correction. Compared with the other prior TIADC time-skew calibrations, our work has a faster convergence time, reduces hardware resources, and does not have intensive computation.

The simulation results demonstrate that the proposed method significantly reduces the BER and enhances the robustness of the circuit system. The effectiveness of these techniques is evaluated by measuring the system's overall performance using BER for a specific realistic system setup. In conclusion, the proposed OFDM–TIADC communication structure and calibration technique offer a robust method to address the issue of TIADC mismatches.

## REFERENCES


[1] S. D. Dissanayake and J. Armstrong, "Comparison of ACO-OFDM, DCO-OFDM and ADO-OFDM in IM/DD systems," *J. Lightw. Technol.*, vol. 31, no. 7, pp. 1063–1072, Apr. 1, 2013.

[2] H. Shen, D. John, and B. Cardiff, "A background calibration for joint mismatch in the OFDM system with time-interleaved ADC," *IEEE Trans. Circuits Syst. II, Exp. Briefs*, vol. 69, no. 9, pp. 3630–3634, Sep. 2022.

[3] Y. Oh and B. Murmann, "System embedded ADC calibration for OFDM receivers," *IEEE Trans. Circuits Syst. I, Reg. Papers*, vol. 53, no. 8, pp. 1693–1703, Aug. 2006.

[4] S. Ponnuru, M. Seo, U. Madhow, and M. Rodwell, "Joint mismatch and channel compensation for high-speed OFDM receivers with time-interleaved ADCs," *IEEE Trans. Commun.*, vol. 58, no. 8, pp. 2391–2401, Aug. 2010.

[5] V.-T.-D. Huynh, N. Noels, and H. Steendam, "Effect of offset mismatch in time-interleaved ADC circuits on OFDM-BER performance," *IEEE Trans. Circuits Syst. I, Reg. Papers*, vol. 64, no. 8, pp. 2195–2206, Aug. 2017.

[6] V.-T.-D. Huynh, N. Noels, and H. Steendam, "BER evaluation of OFDM systems with joint effect of TI-ADC circuit's gain mismatch and channel estimation error," *IEEE Trans. Commun.*, vol. 67, no. 5, pp. 3612–3623, May 2019.

[7] V.-T.-D. Huynh, N. Noels, and H. Steendam, "Closed-form BER expression for OFDM with the effect of TI-ADC's timing mismatch," in *Proc. 25th Int. Conf. Telecommun. (ICT)*, Jun. 2018, pp. 132–137.

[8] Y. A. Tavares, K.-Y. Lee, and M. Lee, "All-digital bandwidth mismatch calibration of TI-ADCs based on optimally induced minimization," *IEEE Trans. Very Large Scale Integr. (VLSI) Syst.*, vol. 28, no. 5, pp. 1175–1184, May 2020.

[9] S. Chen, L. Wang, H. Zhang, R. Murugesu, D. Dunwell, and A. C. Carusone, "All-digital calibration of timing mismatch error in time-interleaved analog-to-digital converters," *IEEE Trans. Very Large Scale Integr. (VLSI) Syst.*, vol. 25, no. 9, pp. 2552–2560, Sep. 2017.

[10] D. Li, L. Zhao, L. Wang, Y. Shen, and Z. Zhu, "A fast convergence second-order compensation for timing skew in time-interleaved ADCs," *IEEE Trans. Very Large Scale Integr. (VLSI) Syst.*, vol. 30, no. 10, pp. 1558–1562, Oct. 2022.

[11] J. Liu, C.-H. Chan, S.-W. Sin, U. Seng-Pan, and R. P. Martins, "Accuracy-enhanced variance-based time-skew calibration using SAR as window detector," *IEEE Trans. Very Large Scale Integr. (VLSI) Syst.*, vol. 27, no. 2, pp. 481–485, Feb. 2019.

[12] Z. Lu, H. Tang, Z. Ren, R. Hua, H. Zhuang, and X. Peng, "A timing mismatch background calibration algorithm with improved accuracy," *IEEE Trans. Very Large Scale Integr. (VLSI) Syst.*, vol. 29, no. 8, pp. 1591–1595, Aug. 2021.

[13] Z. Lu, W. Zhang, H. Tang, and X. Peng, "A novel two-stage timing mismatch calibration technique for time-interleaved ADCs," *IEEE Trans. Very Large Scale Integr. (VLSI) Syst.*, vol. 31, no. 6, pp. 887–891, Jun. 2023.

[14] Y. Qiu, Y.-J. Liu, J. Zhou, G. Zhang, D. Chen, and N. Du, "All-digital blind background calibration technique for any channel time-interleaved ADC," *IEEE Trans. Circuits Syst. I, Reg. Papers*, vol. 65, no. 8, pp. 2503–2514, Aug. 2018.

[15] J. Matsuno, T. Yamaji, M. Furuta, and T. Itakura, "All-digital background calibration technique for time-interleaved ADC using pseudo aliasing signal," *IEEE Trans. Circuits Syst. I, Reg. Papers*, vol. 60, no. 5, pp. 1113–1121, May 2013.

[16] Y. A. Tavares and M. Lee, "A foreground calibration for M-channel time-interleaved analog-to-digital converters based on genetic algorithm," *IEEE Trans. Circuits Syst. I, Reg. Papers*, vol. 68, no. 4, pp. 1444–1457, Apr. 2021.

[17] S. Liu, L. Zhao, and S. Li, "A novel all-digital calibration method for timing mismatch in time-interleaved ADC based on modulation matrix," *IEEE Trans. Circuits Syst. I, Reg. Papers*, vol. 69, no. 7, pp. 2955–2967, Jul. 2022.

[18] V.-P. Hoang and V.-T. Ta, "Fully digital background calibration of channel mismatches in time-interleaved ADCs using recursive least square algorithm," *AEU Int. J. Electron. Commun.*, vol. 130, Feb. 2021, Art. no. 153574. [Online]. Available: https://www.sciencedirect.com/science/article/pii/S1434841120327783

[19] V.-T. Ta, V.-P. Hoang, V.-P. Pham, and C.-K. Pham, "An improved all-digital background calibration technique for channel mismatches in high speed time-interleaved analog-to-digital converters," *Electronics*, vol. 9, no. 1, p. 73, Jan. 2020. [Online]. Available: https://www.mdpi.com/2079-9292/9/1/73

[20] H. Shen, A. Blaq, D. John, and B. Cardiff, "A foreground mismatch and memory harmonic distortion calibration algorithm for TIADC," *IEEE Trans. Circuits Syst. I, Reg. Papers*, vol. 70, no. 3, pp. 1110–1120, Mar. 2023.

[21] M. El-Chammas and B. Murmann, "General analysis on the impact of phase-skew in time-interleaved ADCs," *IEEE Trans. Circuits Syst. I, Reg. Papers*, vol. 56, no. 5, pp. 902–910, May 2009.

[22] H. Shen and B. Cardiff, "Multi-tone ground truth estimation for ADC testing," in *Proc. 32nd Irish Signals Syst. Conf. (ISSC)*, Jun. 2021, pp. 1–5.

[23] H. Le Duc, D. M. Nguyen, C. Jabbour, P. Desgreys, O. Jamin, and V. T. Nguyen, "Fully digital feedforward background calibration of clock skews for sub-sampling TIADCs using the polyphase decomposition," *IEEE Trans. Circuits Syst. I, Reg. Papers*, vol. 64, no. 6, pp. 1515–1528, Jun. 2017.

[24] H. Le Duc et al., "Hardware implementation of all digital calibration for undersampling TIADCs," in *Proc. IEEE Int. Symp. Circuits Syst. (ISCAS)*, May 2015, pp. 2181–2184.

[25] H. Shen, H. Zheng, D. O'Hare, D. John, and B. Cardiff, "Correcting ADC jitter using DPLL timing error signal," in *Proc. 21st IEEE Interregional NEWCAS Conf. (NEWCAS)*, Jun. 2023, pp. 1–5.

[26] H. Le Duc et al., "All-digital calibration of timing skews for TIADCs using the polyphase decomposition," *IEEE Trans. Circuits Syst. II, Exp. Briefs*, vol. 63, no. 1, pp. 99–103, Jan. 2016.

[27] F. Centurelli, P. Monsurro, and A. Trifiletti, "Efficient digital background calibration of time-interleaved pipeline analog-to-digital converters," *IEEE Trans. Circuits Syst. I, Reg. Papers*, vol. 59, no. 7, pp. 1373–1383, Jul. 2012.

[28] J. Nadal and A. Baghdadi, "Parallel and flexible 5G LDPC decoder architecture targeting FPGA," *IEEE Trans. Very Large Scale Integr. (VLSI) Syst.*, vol. 29, no. 6, pp. 1141–1151, Jun. 2021.

[29] H. Cui, F. Ghaffari, K. Le, D. Declercq, J. Lin, and Z. Wang, "Design of high-performance and area-efficient decoder for 5G LDPC codes," *IEEE Trans. Circuits Syst. I, Reg. Papers*, vol. 68, no. 2, pp. 879–891, Feb. 2021.

[30] P. Kang, Y. Xie, L. Yang, and J. Yuan, "Enhanced quasi-maximum likelihood decoding based on 2D modified min-sum algorithm for 5G LDPC codes," *IEEE Trans. Commun.*, vol. 68, no. 11, pp. 6669–6682, Nov. 2020.

[31] T. K. Devi, E. B. Priyanka, P. Sakthivel, and A. S. Sagayaraj, "Low complexity modified Viterbi decoder with convolution codes for power efficient wireless communication," *Wireless Pers. Commun.*, vol. 122, no. 1, pp. 685–700, Jan. 2022.

[32] M. Shirvanimoghaddam et al., "Short block-length codes for ultra-reliable low latency communications," *IEEE Commun. Mag.*, vol. 57, no. 2, pp. 130–137, Feb. 2019.

[33] S. Haykin, *Communication Systems*, 4th ed. Hoboken, NJ, USA: Wiley, 2000.

[34] *Evolved Universal Terrestrial Radio Access (E-UTRA)*, document 3GPP TS 36.101, 3rd Gener. Partnership Project, Tech. Specification Group Radio Access Network, 2017.

[35] J.-J. Van De Beek, O. Edfors, M. Sandell, S. K. Wilson, and P. O. Borjesson, "On channel estimation in OFDM systems," in *Proc. IEEE 45th Veh. Technol. Conf.*, vol. 2, Jul. 1995, pp. 815–819.

[36] *IEEE Standard for Local and Metropolitan Area Networks—Part 16: Air Interface for Fixed and Mobile Broadband Wireless Access Systems—Amendment for Physical and Medium Access Control Layers for Combined Fixed and Mobile Operation in Licensed Bands*, IEEE Standard 802.16E-2005 and IEEE Standard 802.16-2004/Cor, Amendment and Corrigendum to IEEE Std 802.16-2004, Jan. 2005, pp. 1–822.

[37] M. Patzold, C.-X. Wang, and B. O. Hogstad, "Two new sum-of-sinusoids-based methods for the efficient generation of multiple uncorrelated Rayleigh fading waveforms," *IEEE Trans. Wireless Commun.*, vol. 8, no. 6, pp. 3122–3131, Jun. 2009.

**Haoyang Shen** (Member, IEEE) received the B.E. degree from the University College Dublin, Dublin, Ireland, in 2019, where he is currently working toward the Ph.D. degree.

His current research interests include analog-to-digital converter (ADC) calibration algorithm, digital signal processing, and circuit system design.

**Deepu John** (Senior Member, IEEE) received the B.Tech. degree in electronics and communication engineering from the University of Kerala, Thiruvananthapuram, India, in 2002, and the M.Sc. and Ph.D. degrees in electrical engineering from National University Singapore, Singapore, in 2008 and 2014, respectively.

He worked as a Senior Engineer with Sanyo Semiconductors, Gifu, Japan. He was a Post-Doctoral Researcher with the Bio-Electronics Laboratory, National University Singapore, from 2014 to 2017. He is currently an Assistant Professor with the School of Electrical and Electronics Engineering, University College Dublin, Dublin, Ireland. His research interests include the Internet of Things (IoT)/wearable sensing, biomedical circuits and systems, and edge computing.

Dr. John was a recipient of the Institution of Engineers Singapore Prestigious Engineering Achievement Award in 2011, the Best Design Award at the Asian Solid-State Circuit Conference in 2013, and the IEEE Young Professionals, Region 10 Individual Award in 2013. He has served as a member of the organizing or technical committee for several IEEE conferences, such as ISCAS, BioCAS, NorCAS, ICECS, AICAS, MWSCAS, APCCAS, TENCON, ASICON, and ICTA. He is a reviewer for several IEEE journals and conferences. He has served as an Associate Editor for IEEE TRANSACTIONS ON BIOMEDICAL CIRCUITS AND SYSTEMS and a Guest Editor for IEEE TRANSACTIONS ON CIRCUITS AND SYSTEMS—I: REGULAR PAPERS and IEEE OPEN JOURNAL OF CIRCUITS AND SYSTEMS. He currently serves as a Senior Associate Editor for IEEE TRANSACTIONS ON CIRCUITS AND SYSTEMS—II: EXPRESS BRIEFS and as an Associate Editor for *IEEE Internet of Things Magazine* and *International Journal of Circuit Theory and Applications* (Wiley).

**Barry Cardiff** (Senior Member, IEEE) received the B.Eng. degree from the Electronic Engineering Department, University College Dublin (UCD), Dublin, Ireland, in 1992, the M.Eng.Sc. degree (by research), and the Ph.D. degree in digital signal processing (DSP) for wireless and optical communications from UCD in 2011, under the supervision of Prof. Tony Fagan. His Ph.D. dissertation was titled, "Detection Techniques in Vector Systems in Communications."

He was a Design Engineer with Nokia Mobile Phone (U.K.) Ltd., from 1993 to 2001, working on some of world's more advanced and innovative products culminating in the role of a Chief Engineer and as a contributor to the 3GPP standardization process. Then, he moved to Ireland in 2001 to work as a Systems Architect at Silicon and Software Systems (S3 Group), working mainly on embedded hardware/software development projects with applications ranging from wireless communications to hearing aids. He continued to work for S3 Group for several years after a break between 2007 and 2011 to obtain his Ph.D. degree. In September 2013, he joined UCD, as an Academic Staff, to complement the teaching staff both in Dublin and in a joint collaboration in Beijing (BDIC). His research interests are in the area of DSP applications mainly in communication systems both in the theoretical analysis and practical advancement of such systems, and power/complexity reduction techniques in circuit design, i.e., DSP algorithms for digitally assisted analog circuits.